Journal of Energy Storage 44 (2021) 103384

Contents lists available at ScienceDirect

Journal of Energy Storage

journal homepage: www.elsevier.com/locate/est

Research Papers

Optimum design of a double elliptical latent heat energy storage system during the melting process

Amir Hossein Eisapour [a], Mehdi Eisapour [b,*], Hayder I. Mohammed [c], A.H. Shafaghat [a], Mohammad Ghalambaz [d,e], Pouyan Talebizadehsardari [f,*]

[a] Department of Energy and Aerospace Engineering, School of Mechanical Engineering, Shiraz University, Shiraz, Iran
[b] Department of Chemical and Petroleum Engineering, University of Calgary, 2500 University Drive, NW, Calgary, Alberta, T2N 1N4, Canada
[c] Department of Physics, College of Education, University of Garmian, Kurdistan, Iraq
[d] Metamaterials for Mechanical, Biomechanical and Multiphysical Applications Research Group, Ton Duc Thang University, Ho Chi Minh City, Viet Nam
[e] Faculty of Applied Sciences, Ton Duc Thang University, Ho Chi Minh City, Viet Nam
[f] Centre for Sustainable Energy Use in Food Chains, Institute of Energy Futures, Brunel University London, Kingston Lane, Uxbridge, Middlesex, UB8 3PH, UK

ARTICLE INFO

Keywords:
Latent heat storage
Phase change material
Heat transfer fluid
Elliptical tubes
Melting process
Operating conditions

ABSTRACT

This paper concerns the optimum design of double elliptical latent heat storage units during the charging process using three-dimensional numerical simulation. Water and RT35 are employed as the heat transfer fluid and phase change material, respectively. The orientations of both inner and outer elliptical tubes, the number of inner tubes, and the comparison between the straight and wavy configurations for the inner tubes are examined to find the maximum melting rate. Moreover, the sensitivity analysis on the operating conditions, including the Reynolds number and inlet water temperature, is performed. The results show that the best performance is found when the inner and outer tubes are oriented vertically and horizontally, respectively. The performance of the unit enhances as the distance between the inner tube and the bottom wall of the outer tube reduces. Besides, the optimum place for positioning the inner tube is where the minimum distance of the ellipses is 2 mm. It is found that the implementation of double wavy inner pipes increases the heat transfer surface area, which accelerates the melting time by 2.17. The delivered energy rate to the PCM using double wavy inner tubes is 218.75 W/kg, while it is 180.4 W/kg using double straight inner tubes. Eventually, the sensitivity analysis confirms the system is more sensitive to the variations of inlet temperature compared to the Reynolds number regarding the tested operating conditions.

1. Introduction

Thermal energy storage (TES) has been proven as an efficient solution for balancing the mismatch between energy supply and demand for both heating and cooling [1]. It improves an energy consumption system's performance by smoothing supply and demand and reducing the temperature fluctuations in the system [2]. Accordingly, it is established to store excess energy, which otherwise would be lost [3]. The TES has been employed to store different renewable energies, especially solar energy, which could be utilised when the energy source is not available [4]. It also helps peak-shaving results in CO_2 mitigation [5].

TES can be divided into three main categories, including sensible, latent and thermochemical. Among them, latent heat TES (LHTES) has attracted lots of attention due to its large heat storage capacity compared with the sensible heat storage per unit mass and unit volume by storing heat in the phase change materials (PCM) [6]. One of the other main advantages of LHTES is having heat storage in an almost constant temperature giving an added benefit for the application with higher performance using heat with small temperature differences such as building, heat pumps, ice/water storage, etc. [2]. Nevertheless, the main disadvantage of PCM, which is the low thermal conductivity and low rate of thermal diffusion within the bulk PCM, requires an effective heat transfer enhancement method to reach the desired storage/retrieval rate [7]. There are different enhancement techniques, including employing nanoparticles [8], high conductivity foams [9], geometry modification [10], and fins [11], which can be utilised based on the application, required storage rate, and employed materials [12, 13].

* Corresponding author.
E-mail addresses: a.h.eisapour@gmail.com (A.H. Eisapour), mehdi.eisapourdarzi@ucalgary.ca (M. Eisapour), mohammad.ghalambaz@tdtu.edu.vn (M. Ghalambaz), pouyan.talebizadehsardari@brunel.ac.uk (P. Talebizadehsardari).

https://doi.org/10.1016/j.est.2021.103384
Received 13 January 2021; Received in revised form 28 September 2021; Accepted 29 September 2021
Available online 12 October 2021

Nomenclature

A_m	mushy zone constant
C_p	specific heat transfer, $Jkg^{-1}K^{-1}$
E	energy, J
$\overrightarrow{g}$	gravity acceleration, m s^{-2}
H	total enthalpy, J
k	conductivity, $Wm^{-1}K^{-1}$
L_f	latent heat, J/kg
M	mass, kg
R	radius, m
$\overrightarrow{S}$	source term of momentum, m s^{-1}
S_L	source term of energy, J
T	temperature, K
t	time, s
U_i	velocity components, m s^{-1}
$\overrightarrow{V}$	velocity vector, m s^{-1}
V	volume, m^3

Greek

∇	gradient operator
λ	liquid fraction
μ	viscosity, Pa s
ρ	density, kg m^{-3}

Subscript

i	inner
o	outer
PCM	phase change material
T	total

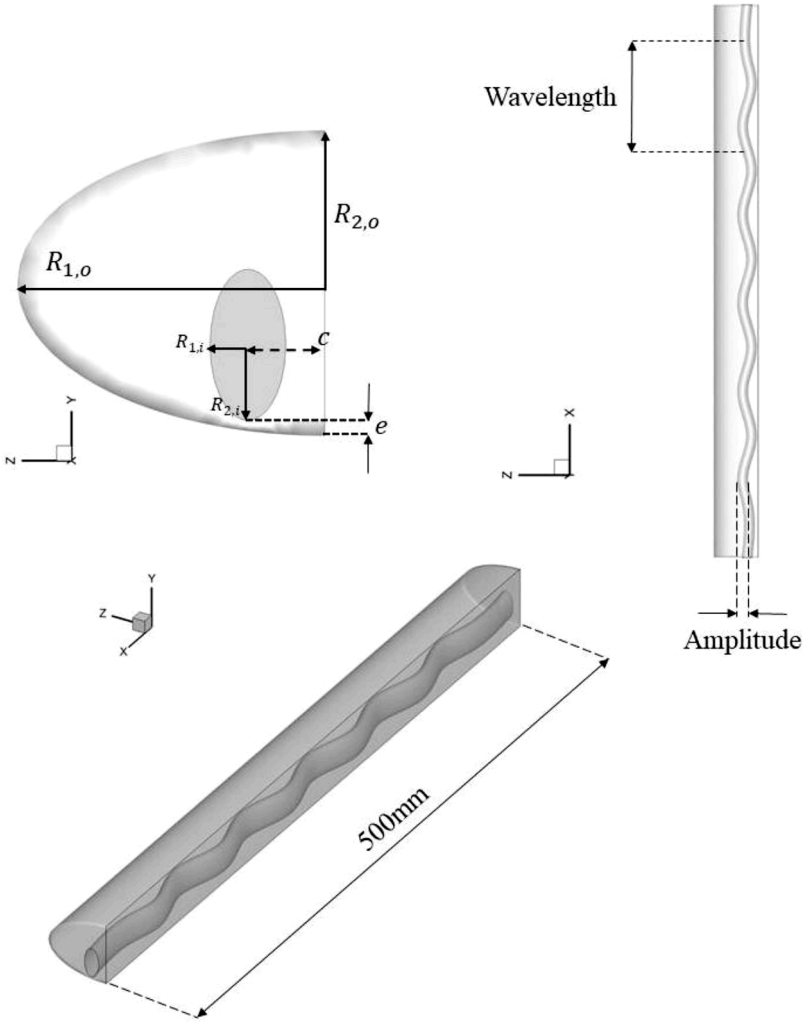

Fig. 1. Dimensional characteristics of the proposed double elliptical heat storage unit.

Geometry modification is an established concept to increase the heat transfer performance to/from the PCMs, which is usually performed by increasing the surface area of heat transfer. Several methods can be considered, including using a higher number of heat transfer fluids (HTF), recirculating the HTF channel, HTF channel modification, and fins addition, which has been examined by several researchers in the literature. As a more efficient enhancement method, triple or even multiple tubes, heat exchangers have recently been more employed. Ravi and Rajasekaran [14] did experimental work on PCM solidification in a triple-tube solar LHTES for the milk industry. Esapour et al. [15] assessed a multi-tube LHTES in comparison with triple-tube and double-tube systems and presented that by employing four inner tubes

Table 1
Dimensional properties of different configurations of studied heat storage units.

	$R_{1,\ o}$	$R_{2,\ o}$	$R_{1,\ i}$	$R_{2,\ o}$	Length	Wave-length	Amplitude	e	c
	(All dimensions are in mm)								
Case 1	40	20	14	7	500	–	–	13	0
Case 2	20	40	7	14	500	–	–	26	0
Case 3	40	20	7	14	500	–	–	6	0
Case 4	20	40	14	7	500	–	–	33	0
Case 5	40	20	7	14	500	–	–	5	0
Case 6	40	20	7	14	500	–	–	4	0
Case 7	40	20	7	14	500	–	–	3	0
Case 8	40	20	7	14	500	–	–	2	0
Case 9	40	20	7	14	500	–	–	1	0
Case 10	40	20	4.95	9.9	500	–	–	2	10
Case 11	40	20	4.90	9.8	500	80	4	2	10

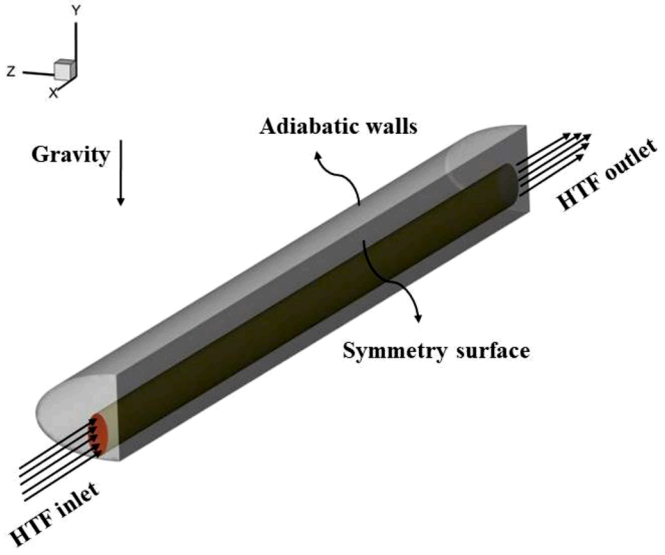

Fig. 2. Computational domain and implemented boundary conditions for case 11.

instead of one, a 29% reduction in the melting time can be achieved. To modify heat transfer, channel waviness is also utilised in heat exchangers by increasing the heat transfer area employed in different applications [16–21]. Nevertheless, limited studies on the literature have been assessed the utilisation of channel waviness. Abdollahzadeh and Esmaeilpour [22] presented the advantages of channel waviness during the solidification process. Shahsavar et al. [23, 24] performed a geometry modification using the application of wavy channels to enhance the heat exchanged from the HTF to/from the PCM. They examined the effects of a constant and variable wave-length of wavy channels in the PCM based double and triple tube LHS systems with and without metal foam application. They showed significant improvement in the melting and solidification mechanisms using geometry modification, even without the presence of metal foams. Mahdi and Nsofor [25] investigated the heat transfer improvement in PCM in a shell-and-tube TES system by arranging multiple conductive foam segments in the PCM to reflect the decay of intensity of heat transfer away from the heat source. They found an enhancement in the energy storage and reduction in the phase changing time using multiple segments.

Modifying the geometry is also performed by adding different types of fins to the heat transfer surface to increase the surface area for heat transfer and distribute the heat source inside the PCM domain. Sciacovelli and Verda [26] numerically studied the effect of the Y-shaped fins in a shell-and-tube LHTES system. They detected that the efficiency of the unit was enhanced by 24%. Also, they claimed that the wide-angle between the branches of the fins is necessary for the short phase change rate. Al-Abidi et al. [27] worked on the PCM melting period in a finned system. They found that the fins thickness has a negligible effect on the phase change rate compared to the length and fins number. Hosseinizadeh et al. [28] investigated the impact of the internal fins in a rectangular heat sink system. They found that the number and the length of the fins considerably improved the efficiency of the unit while changing the thickness provides an insensible effect.

The impact of operating conditions is of paramount importance, especially when a novel system is introduced. The sensitivity analysis of different operating conditions offers a deep insight into the performance of the LHTES in diverse circumstances. Gasia et al. [29] presented an enhancement technique that recirculates the PCM during the charging process. They explored the influence of different operating conditions such as the PCM velocity and flow direction. Their result showed that high PCM velocity leads to an improvement in the charging process of the LHTES. Liang et al. [30] proposed an innovative LHTES with a flat micro-heat pipe array. In their experiments, they performed a sensitivity analysis on various operating parameters, including fluid inlet temperature and velocity. In an experimental study, Raul et al. [31] presented the thermal performance of a vertical shell and tube heat storage unit. They studied the effect of three operating conditions on the HTF outlet temperature in their work; initial PCM temperature, HTF inlet temperature and mass flow rate. Their results indicated that the maximum discharge efficiency of the system is observed when the initial PCM temperature, inlet HTF temperature and mass flow rate is 210 °C, 100 °C and 0.097 kg/s, respectively. Kousha et al. [32] investigated the melting/solidification process in a multitube heat LHTES. They employed water and RT35 as the HTF and PCM, respectively. The inlet temperature of the HTF was set to be 70 °C, 75 °C and 80 °C. For the 4-tube heat storage unit, they found that the time of the melting process reduces by 43% compared to the double pipe heat exchanger. In a numerical study, Pahamli et al. [33] studied the melting behaviour of RT50 employed in a shell and tube LHTES. Their results indicated that despite the fact that escalating the tubes eccentricity and HTF inlet temperature enhances the melting process when both strategies are adopted simultaneously, the impact is more pronounced.

Utilising the PCM has been accompanied by several challenges such as instability and segregation. PCM shows instability when it mixes with some complex materials such as hydrophilic fumed silica, which negatively impacts the mechanical and durability properties [34–37]. Zang et al. [34] examined different paraffin-based stable PCMs fabricated on diatomite, expanded perlite and hydrophilic fumed silica. They stated a considerable amount of PCM leakage (78 wt%) when such PCMs were mixed with cementitious composite. Arias and Wang [38] studied the segregation of particles during the solidification process in the PCM. They showed that the shape factor deeply affects segregation, which means that it can be operated in great scope through modelling and design optimisation.

This study aims to determine the optimal design of a double elliptical latent heat storage system with wavy tubes, which has not been

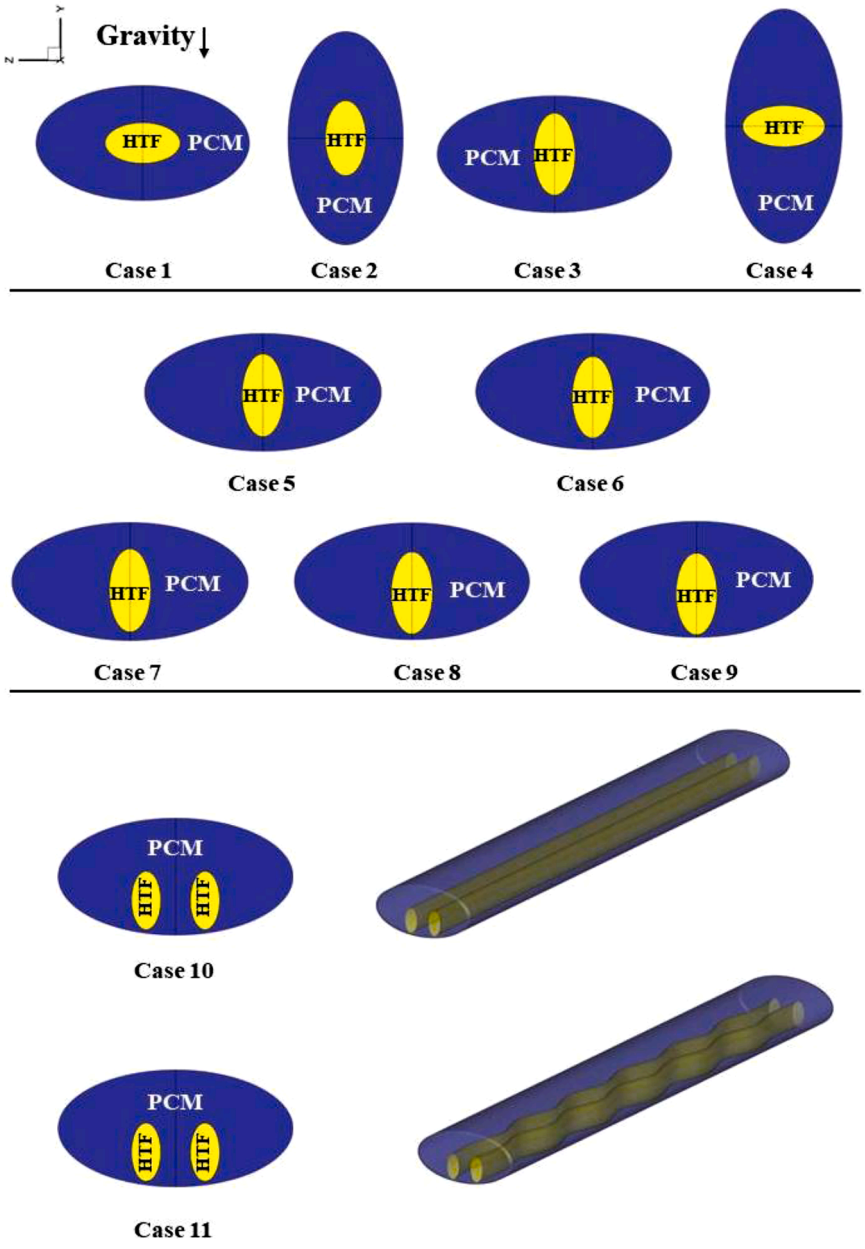

Fig. 3. Different proposed double elliptical heat exchangers.

Table 2
Thermophysical properties of the employed materials in the LHTES units at 298.15 K [43, 44].

	Density (kg/m^3)	Specific heat (J/kg.K)	Thermal conductivity (W/m.K)	Viscosity (kg/m.s)	Latent heat of fusion (J/g)	Thermal expansion (1/K)
RT 35	815	2000	0.20	0.02300	160,000	0.0006
Copper	8960	385	400	–	–	–
Water	996	4072	0.60	0.00086	–	–

conducted so far according to the reviewed literature incorporating both elliptical and wavy tubes in a double-pipe heat exchanger for thermal energy storage. In this way, firstly, the proper distribution of the PCM in a thermal energy storage unit is analysed by varying the orientations of both inner and outer ellipses. Secondly, to take maximum advantage of natural convection, the influence of the inner tube eccentricity is studied. Then, increasing the number of HTF tubes are investigated to extend the surface area of heat transfer (keeping the same mass of the PCM). Moreover, to explore the effect of tube wall profiles in accelerating the melting process, the heat storages with wavy HTF tubes and smooth ones are compared. Eventually, in order to gain a profound insight into the performance of the designed LHTES. Sensitivity analysis on operating conditions is performed. The proposed TES can be employed during the daytime to store thermal energy from the sun and discharge the stored energy during the peak hours for building application where LHTES is preferable due to its capability of providing uniform output temperature

2. System description and boundary conditions

Double elliptical latent heat storage units using smooth and wavy

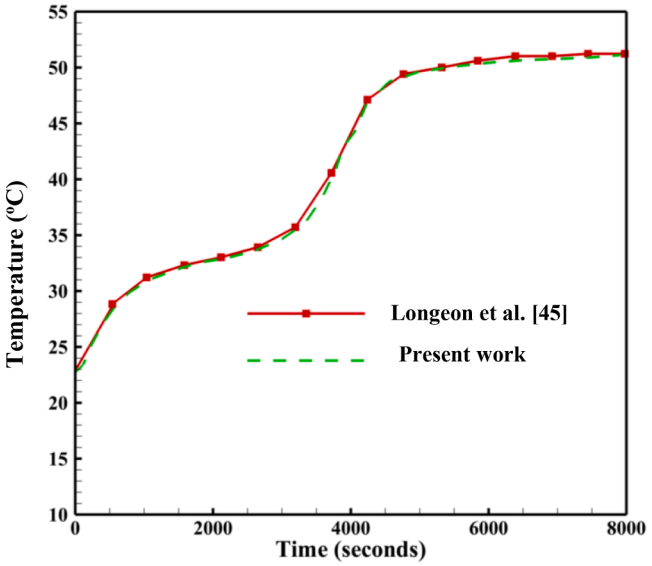

Fig 4. Comparison of melting time between the present work and the study of Longeon et al. [45].

tubes are investigated in the current study. The schematic of the proposed unit is illustrated in Fig. 1. Whereas the heat transfer fluid (HTF) is passed through the inner tube, the outer tube is filled with PCM. As shown in Fig. 1, the length of the heat exchanger in all proposed cases is 500 mm and also several parameters including $R_{1,i}$, $R_{2,i}$, $R_{1,o}$, $R_{2,o}$, e and c are introduced, which show the horizontal and vertical radius of the inner and outer tubes, the minimum distance between the inner and outer tubes, and the horizontal distance between the centre of the inner tube and outer one, respectively. Moreover, wave-length and amplitude are represented in Fig. 1 to illustrate the characteristics of wavy tubes. As can be seen, the distance between successive crests of a wave and the distance moved by a point on the wave from its equilibrium position are defined as wave-length and amplitude, respectively. The geometrical specifications of all 11 configurations investigated in the present work are illustrated in Table 1. To have a similar PCM mass (0.448 kg) in the case with wavy tubes compared with other ones, the HTF tube radius of the wavy cases are changed in proportion as presented in Table 1. It should be noted that the advantages of using elliptical tubes compared with circular tubes in latent heat storage systems was previously studied in the litreture [10]. It was shown that the elliptical tubes enhance the natural convection effect in leatnet heat storage systems and thus, in this paper, elliptical tubes are considered for the inner and outter tubes.

The boundary conditions of the examined heat storage units are depicted in Fig. 2. As it can be observed, the outer walls of the PCM container are considered adiabatic. The contact between the HTF tube and PCM is regarded as a coupled heat transfer boundary (conduction/convection heat transfer). For the HTF, mass flow inlet and mass flow outlet boundary are implemented. Considering the possible application of the proposed LHTES, in all cases, the Reynolds number is 800. Hence, the HTF velocity at the inlet boundary is considered in proportion (approximately 0.01 m/s). Besides, the fluid inlet temperature is 343 K, and the PCM is initialised as a solid at the temperature of 300 K. These situations represent LHTES units incorporating with solar thermal collectors during day times [39]. Since the melting process occurs symmetrically in the gravity direction, only half of the heat storage units are simulated due to the save in time and computational resources.

Fig. 3 represents different configurations of the heat exchanger in the current system. First, the effects of the orientation of both inner and outer tubes are studied in cases 1 to 4, and the best configuration is chosen for further investigations. Then, the concentric heat storage unit is compared with different eccentric ones in cases 5 to 9. In the next step, the effects of increasing the number of HTF tubes are analysed. After this

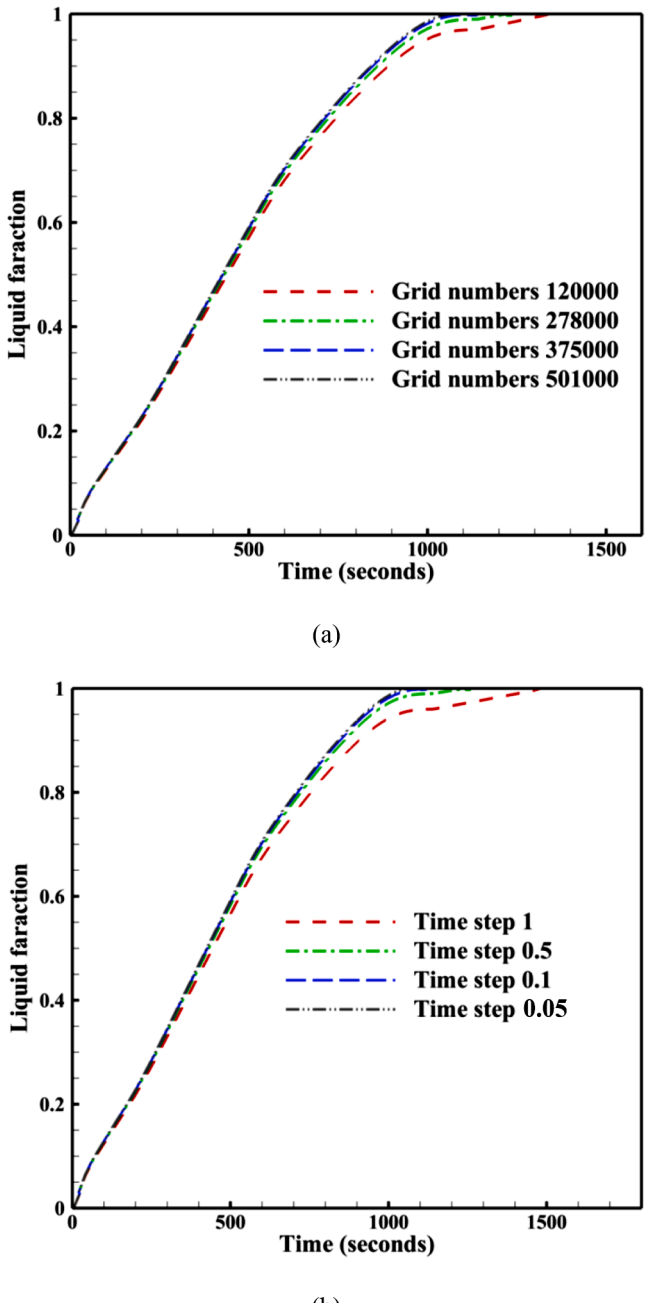

Fig. 5. The results independency from (a) grid numbers (b) time step.

step, the most efficient case in terms of PCM melting time is chosen to study the effect of wavy profile in the heat storage unit, which contains the comparison between cases 10 and 11. To perform a meaningful comparison between these cases, the inlet mass flow rates of all the mentioned cases are the same and also the masses of PCM in different cases are equal to almost 0.5 kg.

3. Governing equations

Three-dimensional models are generated to simulate the phase change phenomenon in the double elliptical latent heat storage unit, and the enthalpy porosity approach is adopted. In all the studied cases, fluid flow is laminar, unsteady, and incompressible. The viscous dissipation is neglected; hence, the flow and temperature distribution can be solved using the conventional Navier-Stokes and the corresponding energy

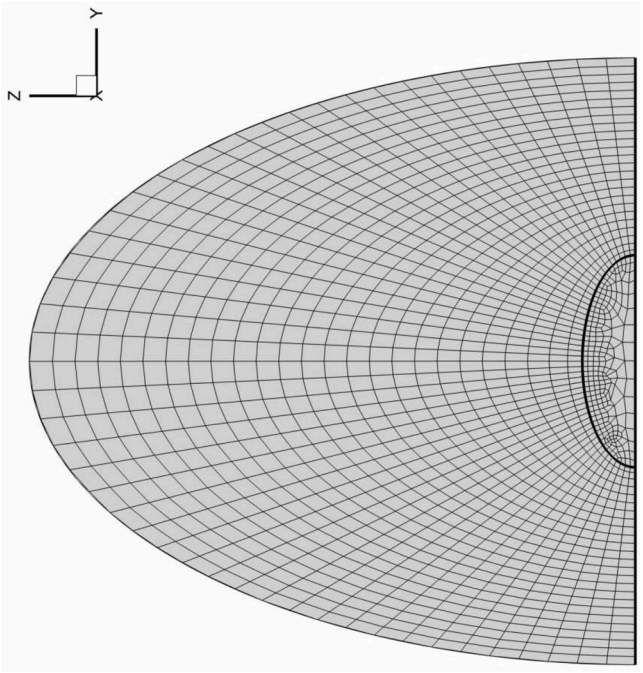

Fig. 6. The generated mesh with 375,000 grids for case 3.

equations, respectively, in the annulus space.

Therefore, the continuity, momentum, and energy equations are expressed as below:

$$\vec{\nabla}.\vec{V} = 0 \tag{1}$$

$$\rho\frac{\partial\vec{V}}{\partial t} + \rho\left(\vec{V}.\vec{\nabla}\right)\vec{V} = -\vec{\nabla}P + \mu\left(\vec{\nabla}^2\vec{V}\right) - \rho\beta\left(T - T_{ref}\right)\vec{g} - \vec{S} \tag{2}$$

$$\frac{\rho C_p\partial T}{\partial t} + \rho\vec{\nabla}\left(C_p\vec{V}T\right) = \vec{\nabla}(k\vec{\nabla}T) - S_L \tag{3}$$

Note that when the PCM is in the liquid state, the flow is considered to be Newtonian, and all PCM properties are constant. To take the natural convection into account, the Boussinesq approximation is applied. The source term $\vec{S}$, which is the damping term of Darcy law, in the momentum equation, is defined as [40]:

$$\vec{S} = A_m\frac{(1-\lambda)^2}{\lambda^3 + 0.001}\vec{V} \tag{4}$$

where A_m is the mushy zone constant which is equal to 10^6 kg/m^3.s. Besides, λ is introduced as; [41]:

$$\lambda = \frac{\Delta H}{L_f} = \begin{Bmatrix} 0 \ if \ T < T_{Solidus} \\ 1 \ if \ T > T_{Liquidus} \\ \dfrac{T - T_{Solidus}}{T_{Liquidus} - T_{Solidus}} \ if \ T_{Solidus} < T < T_{Liquidus} \end{Bmatrix} \tag{5}$$

The source term S_L in the energy equation is obtained as follows:

$$S_L = \frac{\rho\partial\lambda L_f}{\partial t} + \rho\nabla\left(\vec{V}\lambda L_f\right) \tag{6}$$

The total energy of the PCM per unit mass at each time is calculated as:

$$E_T = 1/M_{CPM}\int_{V_{PCM}} EDV \tag{7}$$

where E is the summation of sensible heat (MC_pdT) and latent heat (ML_f) of the PCM. The rate of stored energy during the melting process is then defined as:

$$\dot{E}_T = \frac{E_e - E_i}{t_m} \tag{8}$$

where t_m is the melting time and E_e and E_i are the total energy of the PCM at the end and beginning of the melting process, respectively.

It is worth mentioning that the Reynolds number by which the characteristics of the flow can be realised is expressed as:

$$Re = \frac{\rho Vd}{\mu} \tag{9}$$

Where ρ, V, d and μ are the density of the fluid (kg/m^3), flow speed (m/s), characteristic length (m) and dynamic viscosity of the fluid (kg/(m•s)), respectively.

Copper manufactures the proposed energy storage units to accelerate the heat transfer due to its high thermal conductivity. Note that RT35 is selected as the PCM (melting region 302 K- 309 K) due to its suitability for solar energy applications [42]. The thermophysical properties of RT35, water and copper are illustrated in Table 2. Note that all properties are presented at the standard temperature, which is 298.15 K.

4. Numerical model

To solve the governing equations of the heat storage unit, ANSYS-FLUENT commercial code is employed. The SIMPLEC algorithm is implemented to tackle the pressure-velocity coupling. The gradients of the solved variables at the control volume centre are computed by the Green-Gauss cell-based method. The QUICK differencing scheme is used to solve the momentum and energy equations. Pressure correction equations are solved by adopting the PRESTO scheme. Note that the under relaxation factors are considered to be 0.3, 1, and 0.7 for pressure correction, velocity components, and thermal energy, respectively. It is worth mentioning that the residuals for the convergence of the continuity, momentum, and energy equations are set to be 10^{-4},10^{-4} and 10^{-6}, respectively.

4.1. Validation

Fig. 4 shows the comparison of the calculated liquid fraction plot during the simulation and the experimental study of Longeon et al. [45] to assure the validity of the present study. Longeon et al. [45] investigated an annular LHTES in which RT35 and water were employed as the phase change material and HTF, respectively. Therefore, the experiment and the present work are relatively similar in terms of heat exchanger type and utilised fluids. As shown in Fig. 4, the obtained results in the current study and the experiment of Longeon et al. [45] are in excellent agreement, proving the present simulations' accuracy.

4.2. Grid and time step independency

Various numbers of grids are generated and evaluated to achieve independent results from the mesh. Fig. 5-a illustrates the influence of grid numbers on the time of the melting process for case 3. As shown, for the grid number above 375,000, the results do not vary notably. Therefore, to save computational time, the grid number of 375,000 is selected for further investigations. Fig. 6 represents the structured and refined meshed geometry for case 3 using 375,000 grids selected after grid independence analysis.

To choose a reliable time step, a sensitivity analysis is carried out on different time steps, including 1 s, 0.5 s, 0.1 s, and 0.05 s. As shown in Fig. 5-b, there is no significant difference in the melting time for the time steps 0.05 s and 0.1 s. Hence, 0.1 s is appropriate to reach both reliable results and save computational resources.

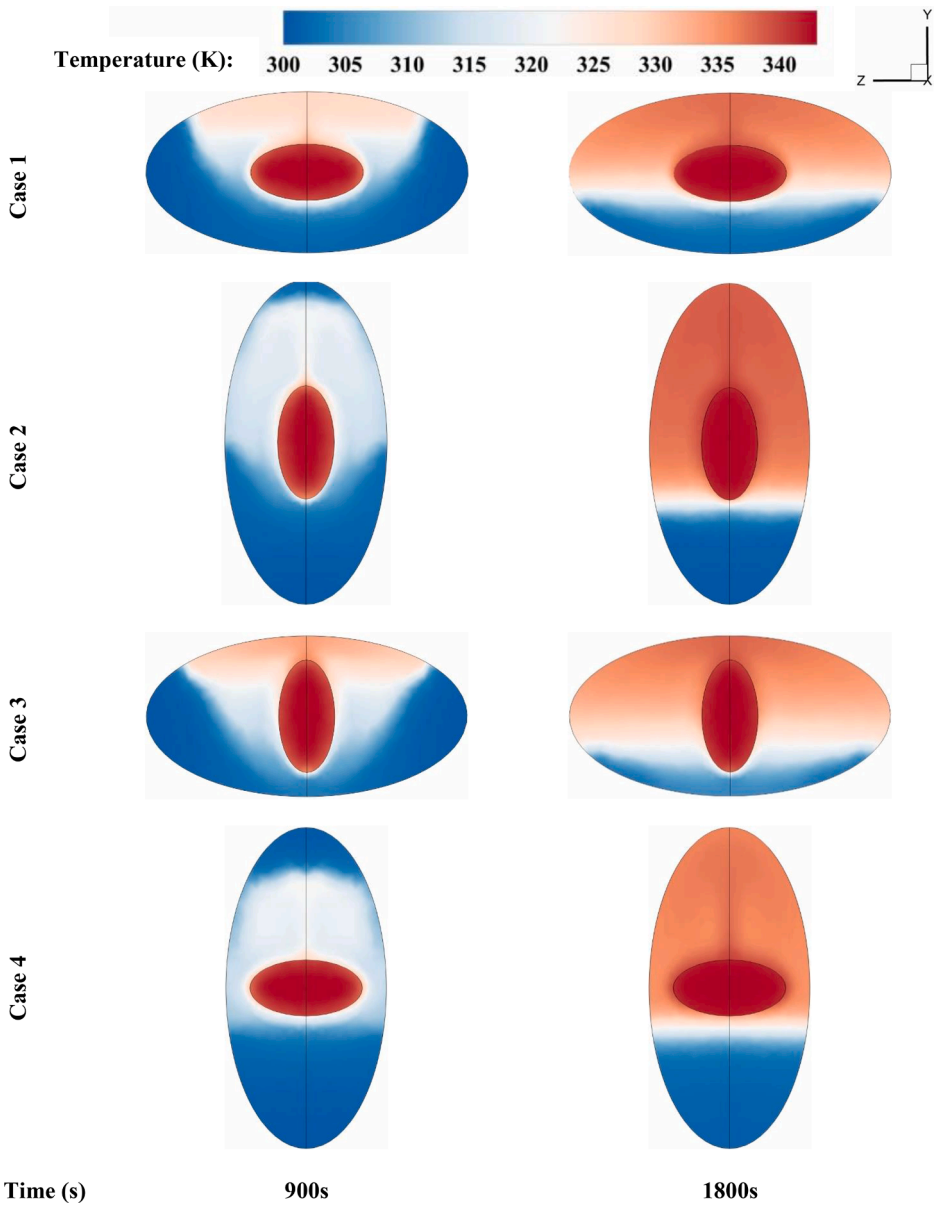

Fig. 7. Temperature contours for cases 1 to 4 after 900 s and 1800s for pure PCM and water as the HTF.

5. Results and discussion

5.1. Effect of elliptical tube orientations

Fig. 7 illustrates the temperature contours of the TES with various positions of the tubes at two different times (900 s and 1800s) during the melting process. Based on this figure, the temperature distributes faster and more uniformly in case 3 compared with the other cases. The reason is that the inner tube, which is the source of the heat, has a larger surface area in the g ravity force direction. The edge of the major diameter of the inner tube is close to the edge of the outer tube's minor diameter, which helps split the PCM into two halves; thus, the convective heat transfers to both sides of the TES equally [10]. Dividing the TES into two parts helps generate two natural circular motions of the molten PCM, leading to faster heat distribution. In other words, in case 3, the proper position of the heat source and the PCM mass distribution allows the LHTES to obtain the most benefit of natural convection. The average temperature of the PCM within the 1800s for cases 1, 2, 3, and 4 are 323.98 K, 323.69 K, 326.52 K, and 323.33 K, respectively.

Fig. 8 shows the liquid fraction contours of the TES with various positions of the tubes at two different times (900 s and 1800s) during the charging process. The PCM begins melting as soon as receiving the conduction heat from the inner tube. The melting process starts with a thin layer of the molten PCM around the inner tube, and then the layer becomes thicker by receiving more heat during the time. The volume of the molten PCM is growing at a different rate depending on the case. Then, the natural convection generates inside the PCM and helps the heat transfer spread in the PCM area, resulting in higher melting fractions [46]. The PCM in case 3 melts faster compared with that in the other cases. As explained previously, the inner tube has a larger surface area in the gravity force direction as the heat source. The edge of the major diameter of the inner tube is close to the minor diameter edge of the outer tube, which divides the PCM domain into two equal regions. As a result, the convective heat transfers to both sides, equally generating more molten PCM. Therefore, the circulating motion of the PCM develops on both sides, helping to mix the molten PCM results in a higher melting rate. Because of the Buoyancy effect, the non-melting PCM was placed at the bottom of the TES. The melting fraction of the PCM within the 1800s in the entire domain for cases 1, 2, 3, and 4 are 0.8106, 0.7608, 0.9357, and 0.6978, respectively. It should be noted that the

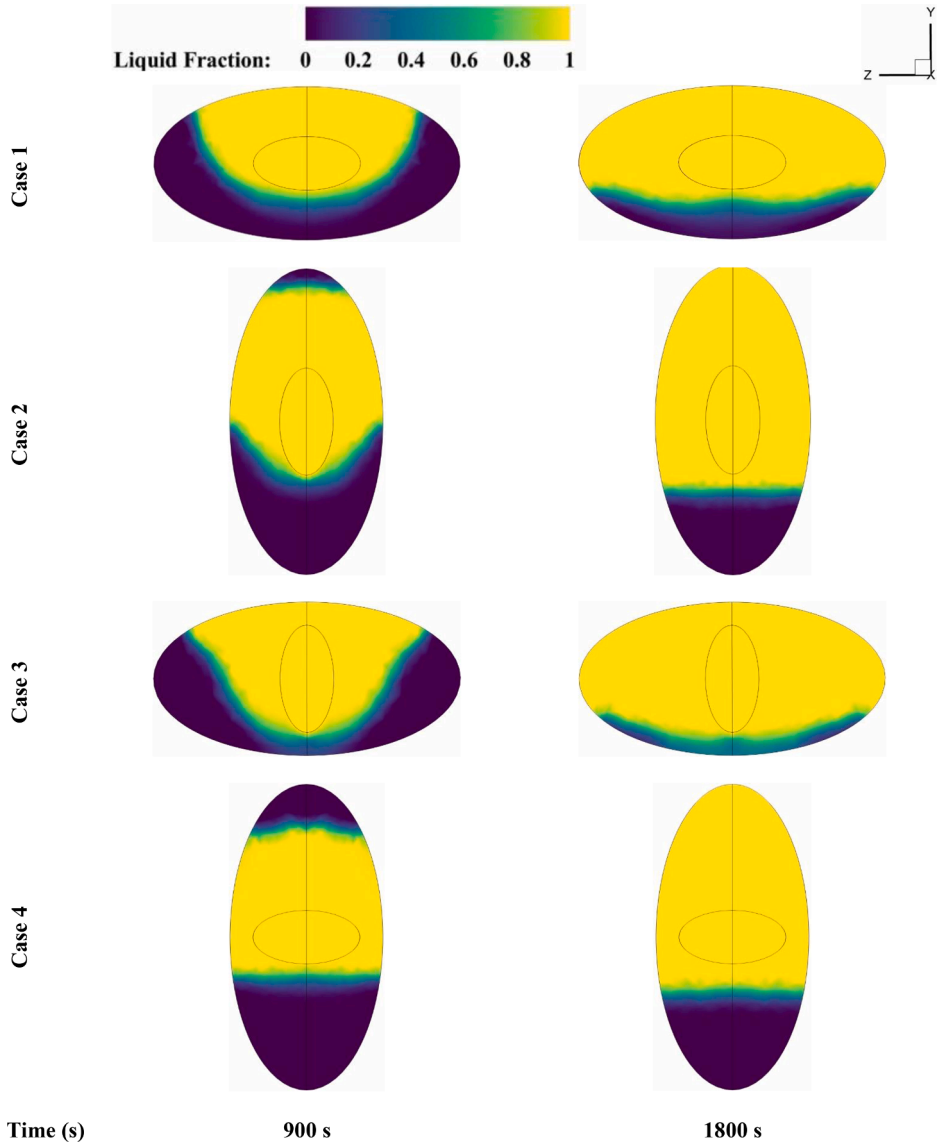

Fig. 8. Liquid fraction contour plots for cases 1 to 4 for pure PCM and water as the HTF after 900 s and 1800s.

melting fraction is calculated at each cell by solving the governing equations. Then, the melting fraction in the entire domain is determined by volume averaging from the melting fraction. Thus, in the charging process, it is concluded that the position of both the inner and outer tubes has a significant impact, and the position of the tubes in case 3 is the best regarding the temperature distribution and melting process.

Fig. 9 illustrates a comparison of the melting process rate for different positions of both inner and outer tubes. As mentioned, the best case regarding the melting rate is case 3. The total PCM melts within the 2440s in case 3, and within 4360 s, 10880s, and 15000s in cases 1, 2, and 4, respectively (melting rate in case 3 is faster than cases 1, 2, and 4 by 1.8, 4.5, and 6.1 times, respectively). The charging rate is maximum when the major axis of the outer tube is horizontal with a major vertical axis of the inner tube, and this process is found to be the slowest for the opposite case (major vertical axis of the outer tube and horizontal axis for the inner tube). The reason is that the close distance between the major axis of the inner and the minor axis of the outer tubes helps to split the PCM into two halves, and as a result, the heat distributes to both sides equally. However, in the opposite case (case 4), the heat does not spread equally due to the convection heat transfer within liquid PCM, leaving the solid-state PCM at the bottom.

Fig. 10 presents the development of the average PCM temperature for various cases with different positions of the inner and outer tubes. The average temperature is considered to compare the cases to realise the temperature distribution through the entire PCM, which is beneficial to evaluate liquid fraction variation as well. The first region is for the first 100 s of the process, in which the temperature rises rapidly (in the stage before the melting) for all cases by a similar trend. The melting starts from region 2, and the cases show slightly different manners for distributing the heat and raising the temperature. From 309 K, region 3 begins, and the cases show different behaviours regarding the temperature. Case 3 rises linearly to convert all the PCM into liquid within 2440s; however, the other cases rise linearly, but at the temperature between 320 and 325 K, the lines get more deviation, which means that the increase in the temperature becomes slower, especially in case 4, which the PCM melts within 15000s.

5.2. *Effect of the tubes' eccentricity*

As case 3 was found to be the best position regarding the melting rate, in the following, this case studied the vertical position of the inner tube. The inner tube slightly moves down in cases 5–9. Fig. 11 shows the temperature distribution in the PCM (left-hand side) and the liquid fraction (right-hand side) at the time of 900 s. The temperature contours

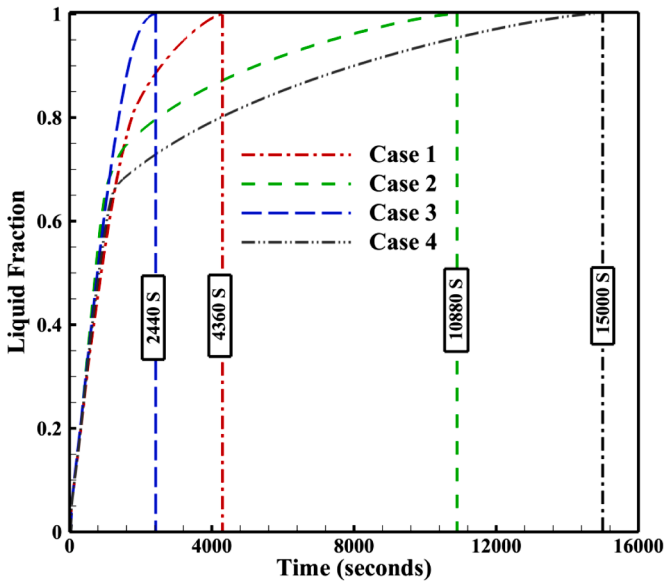

Fig. 9. The influence of elliptical tubes orientations on the liquid fraction.

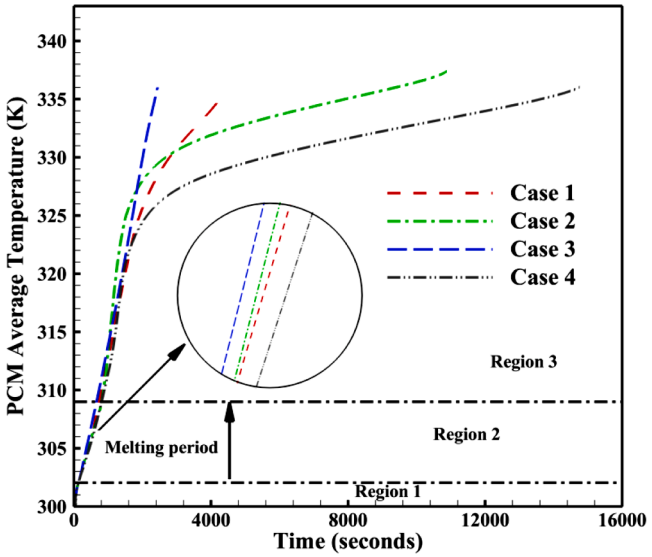

Fig 10. The effect of elliptical tubes orientations on average temperature PCM.

show fewer differences between the maximum and the minimum temperatures in case 8 since the heat source (inner tube) is further to the top part of the outer tube compared with the other cases. The figure shows that there are slight differences in the liquid fraction between cases 5–9.

The existence of the inner tube at the bottom position (case 8) helps to melt the remained solid PCM during the melting time, which exists at the bottom of the domain. This is clearly illustrated in Fig. 12, which shows that the total melting time decreases with closing the inner tube to the outer tube's bottom side. In case 8, the PCM melts within the 1880s. However, it melts within 1900s and 2440s in cases 9 and 3, respectively. It should be noted that the natural convection in the PCM domain enhances by moving the heat source (inner tube) towards the bottom part of the PCM container. This is because placing the heat source at the bottom part of the PCM container results in consistent natural convection assisting the melting process. Nevertheless, the heat source position has an optimum place which is taken in case 8. In this regard, when the distance of the inner and outer tube walls is less than 2 mm (case 9), the charging time increases compared to case 8. The reason is that there is a trade-off between moving the heat source towards the bottom of the LHTES and intensifying the heat transfer inside the storage.

In the optimum positioning scenario of the heat source (case 8), the distance between the lower parts of the HTF tube and the outer tube's wall is used for replacing the cold PCM with a warm one (natural convection phenomenon). When there is not a sufficient distance between the heat source and the outer wall (case 9), the discussed circulation will not take place properly. Thus, to take the most advantage of the convection heat transfer mechanism, the best case in terms of melting rate is case 8; therefore, this case is selected for further investigation.

5.3. *Effect of HTF tube number*

Two more cases are designed based on case 8 using double heat sources (two inner tubes). Case 10 has two straight inner tubes, while case 11 has two wavy inner tubes. Fig. 13 shows the development of the average PCM temperature for cases 8, 10 and 11. The average temperature for the system with wavy inner tubes (case 11) rises more than that for the LHTES with straight tubes. For case 11, the average PCM temperature reaches 335 K within 1135s while it gets to 325 K within the same time in case 10. This behaviour is caused by the large surface area of the wavy tubes, which provides a large heat transfer area between the HTF and the PCM, causing a faster increase in the temperature. Therefore, the PCM in case 11 melts faster. The total PCM melts within 1120s and 1275s in cases 11 and 10, respectively, as shown in Fig. 14.

Fig. 15 shows the PCM total energy per unit mass of the PCM behaviour for cases 8, 10 and 11. The total energy per unit mass has a higher value for the case with wavy tubes than the straight tubes. The total energy of the PCM per unit mass in case 11 is equal to 245 kJ/kg within 1120s, while it is equal to 230 kJ/kg within 1275s for case 10. The reason is that a higher amount of energy transfers to the PCM in the wavy tube case due to the larger surface area for heat transfer. Hence, the transferred energy rate to the PCM using double wavy inner tubes is 218.75 W/kg, while it is 180.4 W/kg using double straight inner tubes.

Fig. 16 shows the temperature distribution on different cross-sections in cases 10 and 11 at 300 s. The temperature of the PCM rises (in the region around the inner tubes) in both cases; however, as shown, a higher increase in the case with wavy tubes (case 11) occurs. By comparing the temperature distribution for the last cross-section for both cases, the region around the inner tubes in case 11 has a higher temperature compared to case 10 since a higher amount of heat is gained in case 11 by the PCM during 300 s. This behaviour shows more clearly in Fig. 17, displaying the temperature distribution within 900 s. The temperature of the PCM in case 11 shows a higher temperature for all cross-sections compared with those in case 10, even in the inlet cross-section; however, for the outlet section, the temperature shows higher values in the wavy tubes system compared with that with straight tubes. This is due to transferring a large amount of energy from the heat source because of the large surface area for the system with wavy tubes.

Fig. 18 shows the liquid fraction (right-hand side) and the flow pattern on the vertical plane on the flow direction (left-hand side) for cases 10 and 11 at times of 300 s and 900 s. The figure illustrates that the liquid fraction is slightly more in case 11, and because of the wavy path, there are three circulation zones, which helps to transfer a higher amount of heat to the PCM. At 900 s, the liquid fraction difference appears more clearly in case 11, and from the left-hand side of the figure, the flow pattern in the wavy tube case shows more condense lines, reflecting the strong flow of the liquid PCM as a result of natural convection.

5.4. *Sensitivity on Reynolds number and HTF inlet temperature*

The sensitivity analysis allows the decision-makers to evaluate the performance of the system in different operating conditions. Hence, after introducing the optimum design for the double elliptical wavy LHTES (case 11), in this section, a sensitivity analysis is performed on

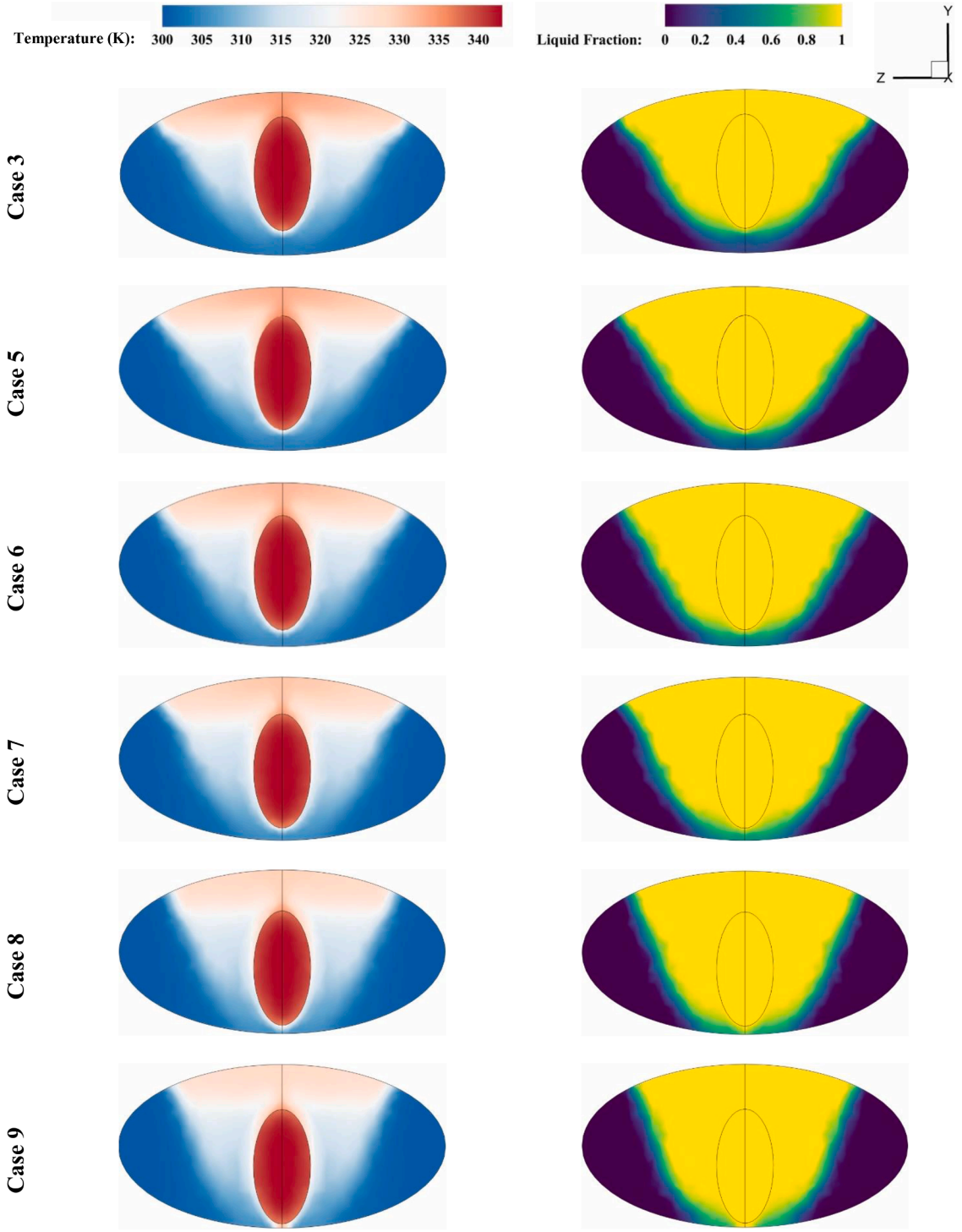

Fig. 11. Liquid fraction and temperature distribution for cases 5–9 after 900 s using pure PCM and water as the HTF.

the impacts of HTF inlet temperature and the Reynolds number. The results for varying the operating conditions of the energy storage unit is illustrated in Fig. 19. It should be noted that the base condition of the system is when the fluid inlet temperature and the Reynolds number is 343 K and 800, respectively. As shown in the figure, by decreasing the HTF inlet temperature and Reynolds number to 338 K and 400, respectively, the charging time escalates by 5% and 12%. In contrast, the increase of 5 K and 800 in HTF inlet temperature and Reynolds number, respectively, leads to the 8% and 12% decline in the charging time of the proposed LHTES. Hence, the increase in Reynolds number and fluid in temperature results in a decrease in melting time, both of which for the rise in the imported energy to the system. Regarding the investigated operating conditions, the system is more sensitive to the variations in HTF inlet temperature compared to that for the Reynolds number.

6. Conclusion

This study investigated in three-dimensional the optimum design of double elliptical latent heat storage units. Different orientations for both inner and outer elliptical pipes were studied in the first step; the best

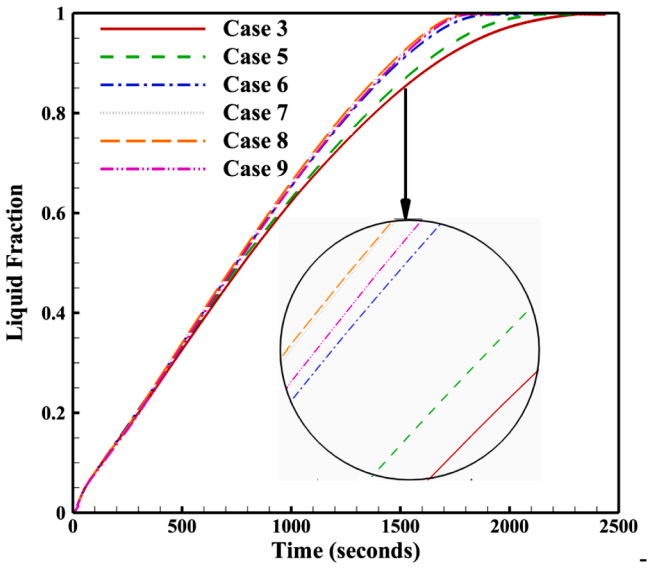

Fig. 12. The effect of tubes eccentricity on the instantaneous liquid fraction of PCM.

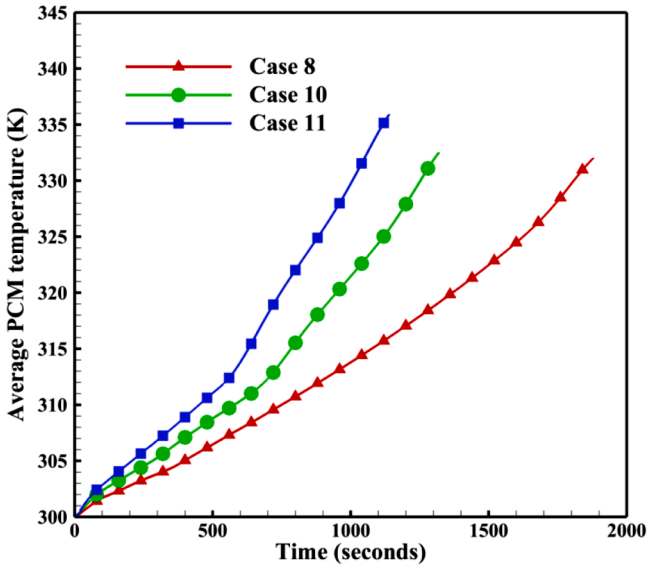

Fig. 13. The average temperature of pure PCM in cases 10 and 11 during the melting process.

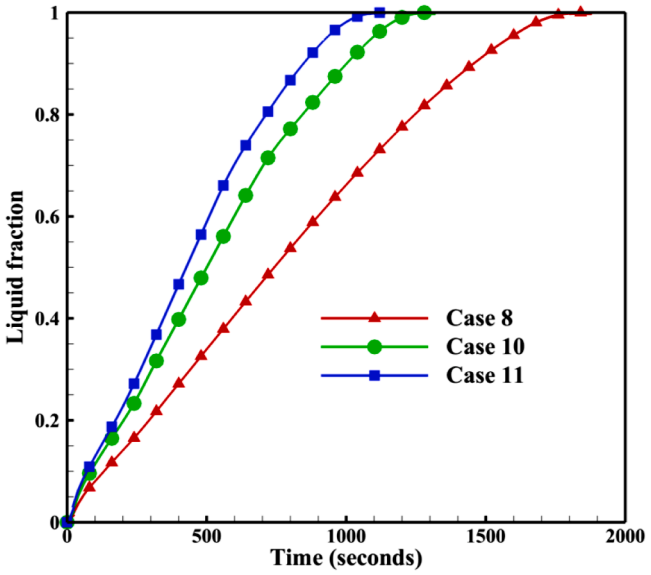

Fig. 14. Instantaneous liquid fraction plot for cases 10 and 11.

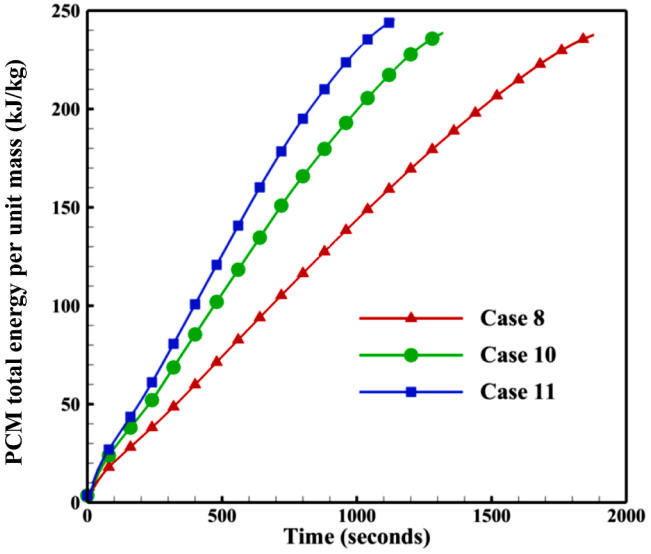

Fig. 15. The total energy of the PCM per unit mass for cases 10 and 11 during the melting process.

developed case was used to find the best position of the inner tube in terms of the heat transfer rate. For the best position selected, double inner tubes with both straight and wavy configurations were studied, showing the system has higher performance with double wavy inner tubes. The optimal position and design were treated with different types and loadings of the nanoparticles used in both HTF and PCM to increase the performance of the melting process. The conclusions drawn from this work are summarised as follows:

- The best orientation of the inner and the outer tubes is the case with a horizontal outer tube and a vertical inner tube (heat source) having a melting time of 2440s. In contrast, the melting time of 15000s is the slowest charging time observed in the case with a vertical outer tube and horizontal inner tube.
- In the best orientations of the tubes, to take the most advantage of the convection heat transfer mechanism, the best position of the inner tube is where it has a 2 mm distance to the bottom wall of the thermal storage container.
- Increasing the number of inner tubes from one to two boosts the melting rate, whereas the PCM melts within 1120s and 1275s when using wavy and straight tubes, respectively.
- The total energy rate delivered to the PCM with the double wavy inner tubes is equal to 218.75 W/kg while it is equal to 180.4 W/kg for the case with a double straight inner tube due to the large surface area.
- The sensitivity analysis on the operational parameters shows a 12% and 5% decrease in the charging time when the Reynolds number and inlet temperature increase by 100% and 1.45%, respectively.

In future studies, the authors will study the effect of orientation and number of elliptical tubes as well as wavy tube implementation during the solidification process. Moreover, other enhancement techniques such as adding nanoparticles inside the PCM and non-uniform distribution of waves are other concepts that are going to be studied for

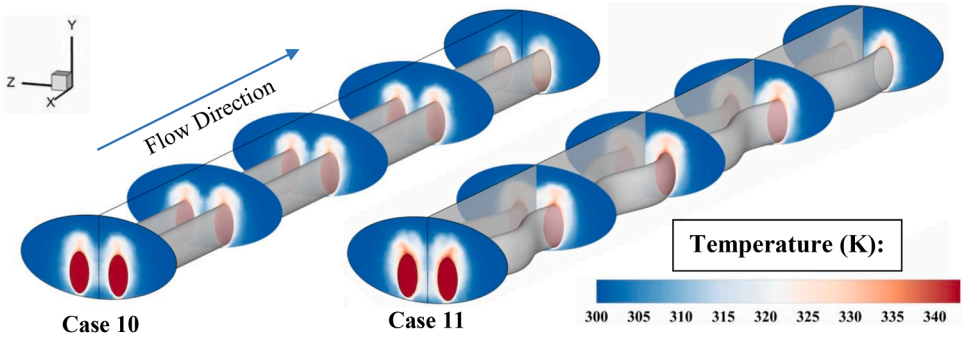

Fig. 16. Temperature contour plot in different cross-sections for cases 10 and 11 after 300 s.

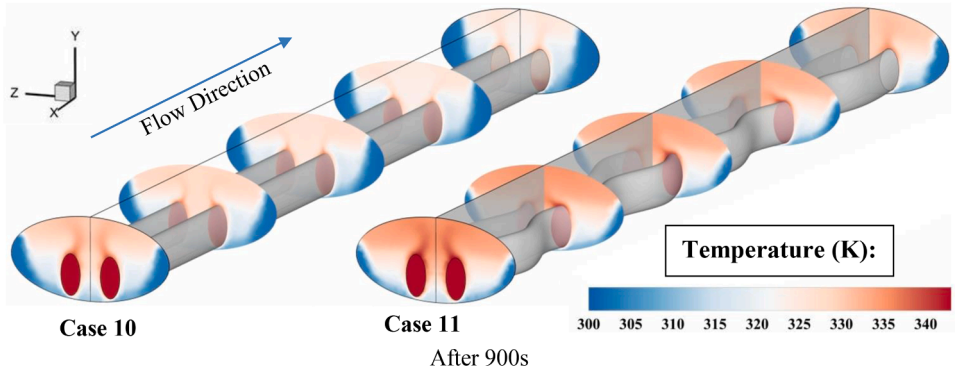

Fig. 17. Temperature contour plot in different cross-sections for cases 10 and 11 after 900 s.

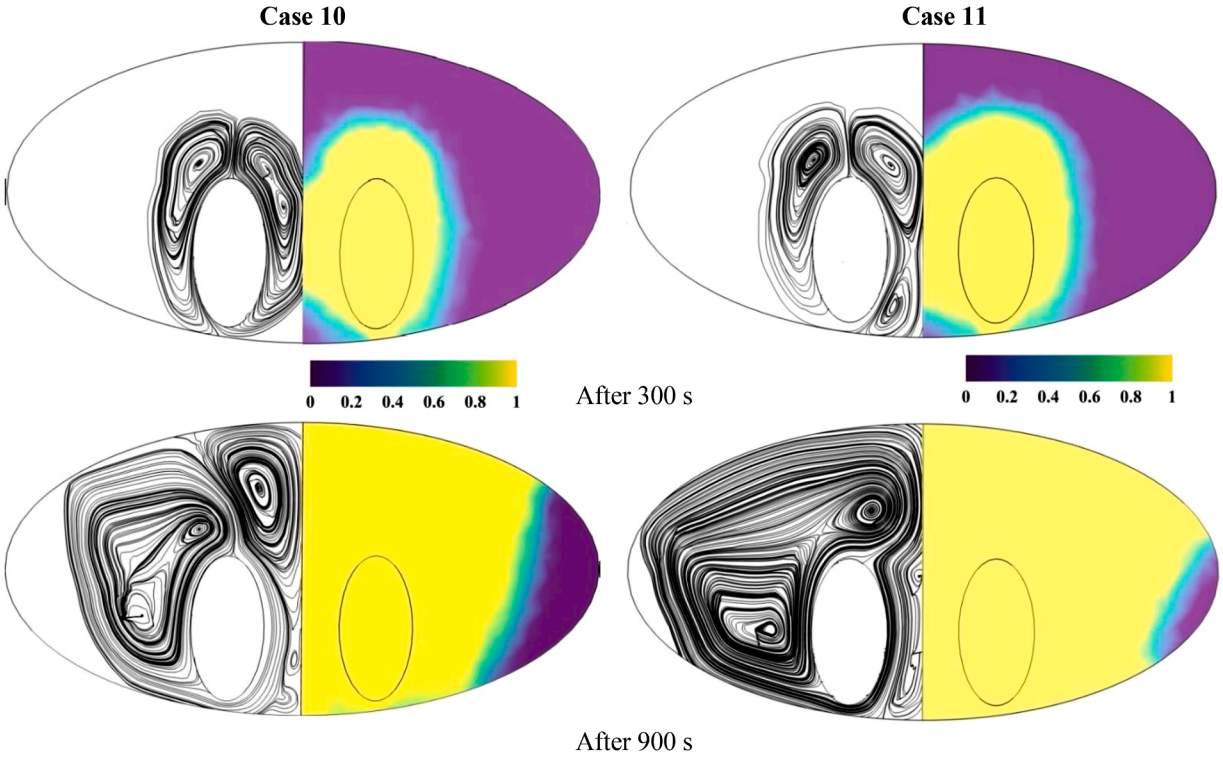

Fig. 18. Liquid fraction contour plot and streamlines for cases 10 and 11 after 300 s and 900 s.

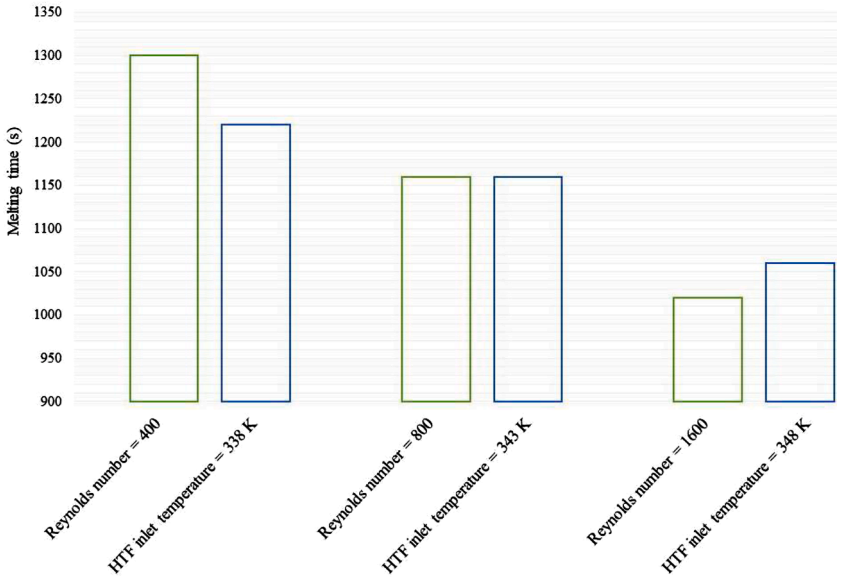

Fig. 19. Sensitivity analysis on Reynolds number and HTF inlet temperature for case 11.

further investigations.

Declaration of Competing Interest

I hereby confirm that there are no known conflicts of interest associated with this publication. All the authors confirm that the manuscript has been read and approved by all named authors and that there are no other persons who satisfied the criteria for authorship but are not listed.

References

[1] L.F. Cabeza, Advances in Thermal Energy Storage systems: Methods and Applications, Elsevier, 2014.
[2] D. Energy, Evidence gathering: Thermal Energy Storage (TES) Technologies, Department for Business, Energy & Industrial Strategy, 2016. Technical Report.
[3] P.T. Sardari, D. Grant, D. Giddings, G.S. Walker, M. Gillott, Composite metal foam/PCM energy store design for dwelling space air heating, Energy Convers. Manage. 201 (2019), 112151.
[4] I. Dincer, M. Rosen, Thermal Energy storage: Systems and Applications, John Wiley & Sons, 2002.
[5] H. Paksoy, H. Evliya, S. Bozdag, M. Mazman, Y. Konuklu, B. Turgut, O. Gok, M. Yilmaz, S. Yilmaz, B. Beyhan, CO2 mitigation with thermal energy storage, Int. J. Glob. Warm. 1 (2009) 253–269.
[6] S. Hasnain, Review on sustainable thermal energy storage technologies, Part I: heat storage materials and techniques, Energy Convers. Manage. 39 (1998) 1127–1138.
[7] L. Fan, J.M. Khodadadi, Thermal conductivity enhancement of phase change materials for thermal energy storage: a review, Renew. Sustainable Energy Rev. 15 (1) (2011) 24–46.
[8] A. Shahsavar, M. Eisapour, P. Talebizadehsardari, Experimental evaluation of novel photovoltaic/thermal systems using serpentine cooling tubes with different cross-sections of circular, triangular and rectangular, Energy 208 (2020), 118409.
[9] M. Esapour, A. Hamzehnezhad, A.A.R. Darzi, M. Jourabian, Melting and solidification of PCM embedded in porous metal foam in horizontal multi-tube heat storage system, Energy Convers. Manage. 171 (2018) 398–410.
[10] H. Bazai, M. Moghimi, H.I. Mohammed, R. Babaei-Mahani, P. Talebizadehsardari, Numerical study of circular-elliptical double-pipe thermal energy storage systems, J. Energy Storage 30 (2020), 101440.
[11] M.E. Tiji, M. Eisapour, R. Yousefzadeh, M. Azadian, P. Talebizadehsardari, A numerical study of a PCM-based passive solar chimney with a finned absorber, J. Build. Eng. 32 (2020), 101516.
[12] L. Yang, J.-n. Huang, F. Zhou, Thermophysical properties and applications of nano-enhanced PCMs: an update review, Energy Convers. Manage. 214 (2020), 112876.
[13] Z. Li, A. Shahsavar, A.A.A.A. Al-Rashed, P. Talebizadehsardari, Effect of porous medium and nanoparticles presences in a counter-current triple-tube composite porous/nano-PCM system, Appl, Therm, Eng 167 (2020), 114777.
[14] R. Rengarajan, K. Rajasekaran, Experimental study of solidification of paraffin wax in solar based triple concentric tube thermal energy storage system, Therm. Sci. 22 (2018) 973–978.
[15] M. Esapour, M.J. Hosseini, A.A. Ranjbar, R. Bahrampoury, Numerical study on geometrical specifications and operational parameters of multi-tube heat storage systems, Appl. Therm. Eng. 109 (2016) 351–363.
[16] J.-.Y. Jang, L.-.K. Chen, Numerical analysis of heat transfer and fluid flow in a three-dimensional wavy-fin and tube heat exchanger, Int, J, Heat Mass Transf 40 (1997) 3981–3990.
[17] S.N. Kondepudi, D.L. O'Neal, Frosting performance of tube fin heat exchangers with wavy and corrugated fins, Exp. Therm. Fluid Sci. 4 (1991) 613–618.
[18] R.K. Shah, D.P. Sekulic, Fundamentals of Heat Exchanger Design, Wiley, 2003.
[19] Q. Wang, M. Zeng, T. Ma, X. Du, J. Yang, Recent development and application of several high-efficiency surface heat exchangers for energy conversion and utilisation, Appl. Energy 135 (2014) 748–777.
[20] B. Lotfi, B. Sundén, Q. Wang, An investigation of the thermo-hydraulic performance of the smooth wavy fin-and-elliptical tube heat exchangers utilising new type vortex generators, Appl. Energy 162 (2016) 1282–1302.
[21] S. Kashani, A. Ranjbar, M. Abdollahzadeh, S. Sebti, Solidification of nano-enhanced phase change material (NEPCM) in a wavy cavity, Heat Mass Transf. 48 (2012) 1155–1166.
[22] M. Abdollahzadeh, M. Esmaeilpour, Enhancement of phase change material (PCM) based latent heat storage system with nano fluid and wavy surface, Int. J. Heat Mass Transf. 80 (2015) 376–385.
[23] A. Shahsavar, J. Khosravi, H.I. Mohammed, P. Talebizadehsardari, Performance evaluation of melting/solidification mechanism in a variable wave-length wavy channel double-tube latent heat storage system, J. Energy Storage 27 (2020), 101063.
[24] A. Shahsavar, A. Shaham, P. Talebizadehsardari, Wavy channels triple-tube LHS unit with sinusoidal variable wave-length in charging/discharging mechanism, Int. Commun. Heat Mass Transfer 107 (2019) 93–105.
[25] J.M. Mahdi, E.C. Nsofor, Multiple-segment metal foam application in the shell-and-tube PCM thermal energy storage system, J. Energy Storage 20 (2018) 529–541.
[26] A. Sciacovelli, F. Gagliardi, V. Verda, Maximisation of performance of a PCM latent heat storage system with innovative fins, Appl. Energy 137 (2015) 707–715.
[27] A.A. Al-Abidi, S. Mat, K. Sopian, M. Sulaiman, A.T. Mohammad, Internal and external fin heat transfer enhancement technique for latent heat thermal energy storage in triplex tube heat exchangers, Appl. Therm. Eng. 53 (2013) 147–156.
[28] S. Hosseinizadeh, F. Tan, S. Moosania, Experimental and numerical studies on performance of PCM-based heat sink with different configurations of internal fins, Appl. Therm. Eng. 31 (2011) 3827–3838.
[29] J. Gasia, D. Groulx, N.S. Tay, L.F. Cabeza, Numerical study of dynamic melting enhancement in a latent heat thermal energy storage system, J. Energy Storage 31 (2020), 101664.
[30] L. Liang, Y. Diao, Y. Zhao, Z. Wang, F. Bai, Numerical and experimental investigations of latent thermal energy storage device based on a flat micro-heat pipe array–metal foam composite structure, Renew. Energy 161 (2020) 1195–1208.
[31] A.K. Raul, P. Bhavsar, S.K. Saha, Experimental study on discharging performance of vertical multitube shell and tube latent heat thermal energy storage, J. Energy Storage 20 (2018) 279–288.
[32] N. Kousha, M. Rahimi, R. Pakrouh, R. Bahrampoury, Experimental investigation of phase change in a multitube heat exchanger, J. Energy Storage 23 (2019) 292–304.
[33] Y. Pahamli, M.J. Hosseini, A.A. Ranjbar, R. Bahrampoury, Analysis of the effect of eccentricity and operational parameters in PCM-filled single-pass shell and tube heat exchangers, Renew. Energy 97 (2016) 344–357.
[34] P. Zhang, X. Xiao, Z. Ma, A review of the composite phase change materials: fabrication, characterisation, mathematical modeling and application to performance enhancement, Appl. Energy 165 (2016) 472–510.

[35] L.F. Cabeza, H. Mehling, S. Hiebler, F. Ziegler, Heat transfer enhancement in water when used as PCM in thermal energy storage, Appl. Therm. Eng. 22 (2002) 1141–1151.
[36] B. Zalba, J.M. Marın, L.F. Cabeza, H. Mehling, Review on thermal energy storage with phase change: materials, heat transfer analysis and applications, Appl. Therm. Eng. 23 (2003) 251–283.
[37] A. Mills, M. Farid, J. Selman, S. Al-Hallaj, Thermal conductivity enhancement of phase change materials using a graphite matrix, Appl. Therm. Eng. 26 (2006) 1652–1661.
[38] F. Arias, X. Wang, Segregation due to motion of front of solidification in phase change materials systems and dependence with shape and dimension factors, Appl. Therm. Eng. 75 (2015) 366–370.
[39] S. Khanna, K.S. Reddy, T.K. Mallick, Optimisation of solar photovoltaic system integrated with phase change material, Sol. Energy 163 (2018) 591–599.
[40] M. Esapour, M. Hosseini, A. Ranjbar, Y. Pahamli, R. Bahrampoury, Phase change in multi-tube heat exchangers, Renew. Energy 85 (2016) 1017–1025.
[41] P. Wang, X. Wang, Y. Huang, C. Li, Z. Peng, Y. Ding, Thermal energy charging behaviour of a heat exchange device with a zigzag plate configuration containing multi-phase-change-materials (m-PCMs), Appl. Energy 142 (2015) 328–336.
[42] S. Khanna, K. Reddy, T.K. Mallick, Optimisation of solar photovoltaic system integrated with phase change material, Sol. Energy 163 (2018) 591–599.
[43] M. Esapour, M. Hosseini, A. Ranjbar, R. Bahrampoury, Numerical study on geometrical specifications and operational parameters of multi-tube heat storage systems, Appl. Therm. Eng. 109 (2016) 351–363.
[44] Y. Khanjari, F. Pourfayaz, A. Kasaeian, Numerical investigation on using of nanofluid in a water-cooled photovoltaic thermal system, Energy Convers. Manage. 122 (2016) 263–278.
[45] M. Longeon, A. Soupart, J.F. Fourmigué, A. Bruch, P. Marty, Experimental and numerical study of annular PCM storage in the presence of natural convection, Appl. Energy 112 (2013) 175–184.
[46] N. Hajighafoori Boukani, A. Dadvand, A.J. Chamkha, Melting of a Nano-enhanced Phase Change Material (NePCM) in partially-filled horizontal elliptical capsules with different aspect ratios, Int. J. Mech. Sci. 149 (2018) 164–177.